International Journal of Automotive Technology, Vol. 21, No. 2, pp. 351–360 (2020)
DOI 10.1007/s12239–020–0033–8

pISSN 1229–9138/ eISSN 1976–3832

PARTIAL AND FULL BRAKING ALGORITHM ACCORDING TO TIME-TO-COLLISION FOR BOTH SAFETY AND RIDE COMFORT IN AN AUTONOMOUS VEHICLE

Jong-Jin Bae#, Min-Su Lee# and Namcheol Kang*

School of Mechanical Engineering, Kyunpook National University, Daegu 41566, Korea

(Received 11 June 2018; Revised 30 October 2018; Accepted 31 May 2019)

ABSTRACT–In this study we developed an autonomous braking algorithm to satisfy both safety and ride comfort of a vehicle. The proposed algorithm is composed of two-step braking strategies depending on the value of time-to-collision. The first step is a partial braking strategy to provide not only deceleration but also good ride comfort in a normal braking situation, and the second step is a full braking strategy to avoid forward collisions in an emergency braking situation. Further, the partial braking is divided into a recovery and a release zones. The former is to apply braking pressures for the safe deceleration, whereas the latter is to release the braking pressure smoothly for good ride comfort. To determine the partial braking pressures, the nonlinear characteristics of the tire friction is considered and the linear momentum of a preceding vehicle is calculated based on the extrapolation of its motion. Computer simulations using CarSim were executed combined with MATLAB/ Simulink to implement the driving situations, and finally we obtained successful performances satisfying ride comfort as well as safety of the vehicle.

KEY WORDS : Adaptive cruise control, Autonomous braking system, Ride comfort, Simulation

1. INTRODUCTION

An active safety system (ASS) is a vehicle control system developed to help drivers avoid and reduce the severity of accidents. Because more than 60 % of automobile accidents are forward or rear-end collisions (NHTSA, 2018), studies on ASSs to avoid such collisions have been actively conducted. For example, a collision warning/ collision avoidance (CW/CA) system gives the driver a visual or audible signal of the collision risk and controls the vehicle to avoid collisions through autonomous steering or braking. In studying these systems, the time to collision (TTC) is a frequently used indicator for determining when the intervention is required for vehicle control (Isermann and Schmitt, 2012; Yang *et al*., 2017). By controlling the driving situation using the TTC, it is possible to secure the safety of the vehicle and to further improve the ride comfort.

The TTC is the time when a collision is expected between the preceding and following vehicles. Because the TTC is calculated using the relative motion between the two vehicles, it provides reliable information on the risk of collision in actual driving. The TTC is considered a key safety indicator along with the time headway, and it was analyzed to determine the safety impacts in different traffic situations (Vogel, 2003). Moreover, TTC has been used in various ways in autonomous vehicle control because it is a quantitative indicator for the risk of collision (Moon and Yi, 2008; Hayashi *et al*., 2012). Also, the benefits of the CW/CA system using TTC for rear-end collision were studied (Kusano and Gabler, 2012).

In the study of ASS related to braking, it is essential to consider the friction characteristics of the tire, which is the only component in contact with the road surface. The friction between the tire and road has a nonlinear property because of inherent slip characteristics (Savaresi and Tanelli, 2010). Because the estimation of the tire-road friction coefficient is an important research topic enabling prediction of the braking distance, many studies have been conducted to estimate the friction coefficient using the tire slip. For example, a Kalman filter was used to estimate the friction coefficient in real time based on the tire slip but it was not confirmed whether the proposed method could be applied to various tire types (Gustafsson, 1997). In addition, studies have been performed to estimate the friction coefficient by using the tire slip angle considering lateral dynamics (Hahn *et al*., 2002; Erdogan *et al*., 2011). In one study, the lateral deflection of a tire, measured by a piezoelectric sensor, was used to estimate the friction coefficient (Erdogan *et al*., 2011). In another study, the position data of the vehicle measured with a GPS and a gyroscope sensor were used to estimate the friction coefficient (Hahn *et al*., 2002). The friction coefficient

**Corresponding author*. e-mail: nckang@knu.ac.kr
# These authors contributed equally to this work.

estimation using lateral dynamics has an advantage of not requiring a longitudinal slip, however, it has a disadvantage of being ineffective when the slip angle is small as in the case of straight motion.

Adaptive Cruise Control (ACC), which was developed to improve passenger comfort, is a technology that controls the vehicle at a target speed or maintains the inter-vehicle distance from the preceding vehicle. Various methods for implementing ACC have been attempted. A sliding mode control has been primarily used in ACC research because the control system has high response performance against various disturbances and does not require a complicated control algorithm (Ferrara and Claudio, 2007; Kim *et al*., 2007). In the sliding mode method, however, high jerk can occur at the start or end point of braking because braking and throttle are controlled by the on/off method. For this reason, some studies have been conducted on ACC using smooth braking to lower the amount of vehicle jerk. For example, a braking control system has been proposed that performs braking considering ride comfort when the relative distance to the preceding vehicle is smaller than the reference distance calculated for collision avoidance (Yi and Chung, 2001). In addition, a system has been proposed to classify the driving situation of the vehicle considering the tire-road friction characteristics as well as to perform the braking according to the classified driving situation (Wu *et al*., 2009). However, as the vehicle executes braking with the specified deceleration, there is a disadvantage that it cannot respond appropriately to various driving situations. In addition, an ACC using fuzzy control that implements a human driving method as a control algorithm has been performed (Naranjo *et al*., 2003, 2012; Milanés *et al*., 2012), but the characteristics of tires were not considered.

In this study, we propose an autonomous braking algorithm that considers both safety and ride comfort using the TTC. The proposed braking algorithm distinguishes the driving situation between a normal braking situation and an emergency braking situation based on the TTC value and performs appropriate braking according to each situation. Moreover, we used a pressure profile to apply smooth braking for obtaining low jerk of vehicle. In addition, the tire-road friction characteristics were considered when calculating the optimal braking force for the normal braking situation. We evaluated the performance of the developed braking algorithm in the simulations using CarSim and MATLAB/Simulink and obtained satisfactory results.

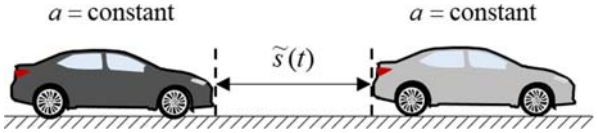

Figure 1. Predicted relative distance to calculate TTC.

2. AUTONOMOUS BRAKING ALGORITHM

This section describes autonomous braking algorithms using TTC. The TTC represents the estimated time to collide between the preceding and following vehicles. Because the TTC implies a risk of collision, it can be used as a criterion in determining whether or not braking is required. Therefore, we classified the driving situation of the vehicle based on the TTC magnitude and adopted two braking strategies suitable for various driving situations to provide a safe and comfortable ride to the passenger. Partial braking, the first braking strategy, was introduced in order to not only prevent collisions but also to apply smooth braking. Full braking, the second braking strategy, was devised to cope with an emergency situation.

2.1. Braking Strategy Using TTC

The TTC is calculated based on the relative motion of both vehicles. Because the TTC is the time when the relative distance between preceding and following vehicles is expected to be zero, it is necessary to predict the relative distance for the calculation of TTC. The relative distance was calculated from the displacement, velocity, and acceleration of the two vehicles. The motion data of the preceding vehicle could be obtained using a vision sensor (Sivaraman and Trivedi, 2013) or V2X technology (Sengupta *et al*., 2007). When both vehicles move at a constant acceleration, the predicted relative distance is written as follows.

$$\tilde{s}(t) = \tilde{s}_0 + \tilde{v}_0 t + \frac{1}{2}\tilde{a}_0 t^2 \tag{1}$$

where $\tilde{s}_0$, $\tilde{v}_0$, and $\tilde{a}_0$ are the measured relative displacement, velocity, and acceleration between the preceding and following vehicles, respectively. The tilde symbol indicates a relative quantity between the two cars and the subscript 0 means that the data is obtained at the time of each calculation point. The relative quantities are values obtained by subtracting the following vehicle from the preceding vehicle. The $\tilde{s}(t)$ function is the predicted relative distance, which is defined as the distance from the rear-end of the preceding vehicle to the front-end of the following vehicle, as shown in Figure 1.

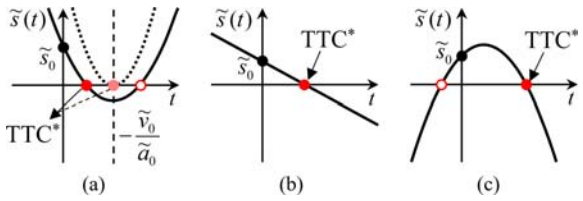

Figure 2. Visualization of cases where TTC* is existed according to relative acceleration between two vehicles: (a) When the relative acceleration is positive, (b) When the relative acceleration is zero, and (c) When the relative acceleration is negative.

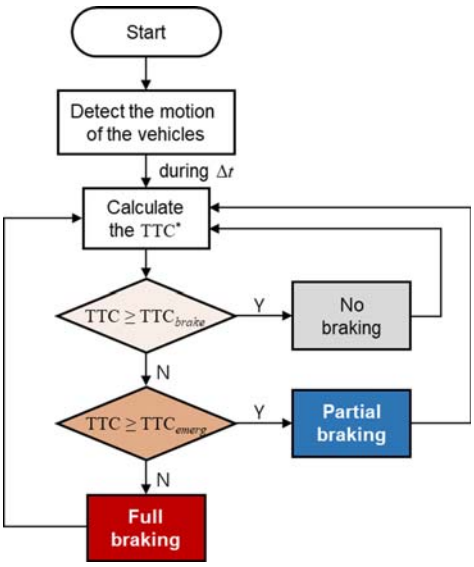

Figure 3. Flow chart of the proposed braking algorithm.

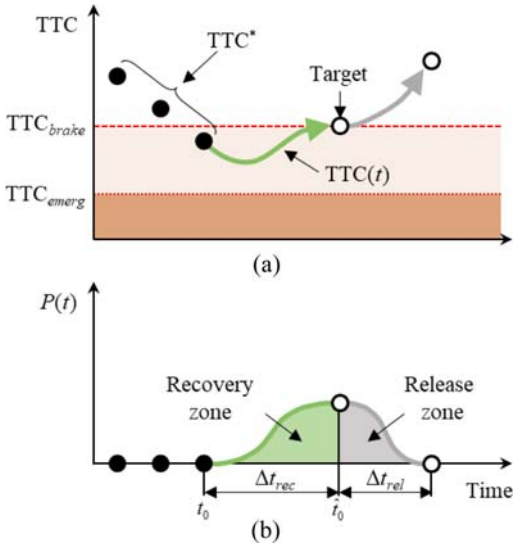

Figure 4. Conceptual diagram of the partial braking algorithm: (a) TTC*; (b) Corresponding brake pressure.

The TTC can be determined mathematically by obtaining the real roots of Equation (1). Among the real roots of Equation (1), the negative root has no physical meaning because it would indicate that the vehicle collided in the past. Therefore, only the real positive root was used in this study. The mathematically determined real positive root in Equation (1) is defined as TTC*. The cases where TTC* exists are classified into three categories according to the value of $\tilde{a}_0$ (see Figure 2). The first category is when $\tilde{a}_0$ is greater than zero. If the vehicles do not collide, $\tilde{s}_0$ is always greater than zero. Therefore, the central axis of $\tilde{s}(t)$ needs to be positive (i.e., $\tilde{v}_0$ should be negative) and the discriminant should be greater than or equal to zero in order to exist a real positive root of Equation (1). Then, if the discriminant is greater than zero, there are two distinct roots in Equation (1). In this case, the minimum value that indicates the first collision time should be selected as the TTC*. Furthermore, if the discriminant is zero, Equation (1) has one multiple root that should be selected as the TTC*. The second category is when $\tilde{a}_0$ is zero. In this case, as is a linear function and $\tilde{s}_0$ is always larger than zero, $\tilde{v}_0$ should be a negative value for a real positive root to exist. The third category is when $\tilde{a}_0$ is less than zero. Because $\tilde{s}_0$ is greater than zero, Equation (1) has one real positive root and one real negative root. Therefore, TTC* will always exist for this case. Using the quadratic formula, it was confirmed that the equations for TTC* in the first and third cases were the same. As a result, TTC* can be written as follows.

$$\mathrm{TTC}^* = \begin{cases} \dfrac{-\tilde{v}_0 - \sqrt{\tilde{v}_0^{\,2} - 2\tilde{a}_0\tilde{s}_0}}{\tilde{a}_0}, & \text{if } (\tilde{a}_0 > 0 \text{ and } \tilde{v}_0 \le -\sqrt{2\tilde{a}_0\tilde{s}_0}) \\ & \text{or } \tilde{a}_0 < 0 \\ -\dfrac{\tilde{s}_0}{\tilde{v}_0}, & \text{if } \tilde{a}_0 = 0 \text{ and } \tilde{v}_0 < 0 \end{cases} \quad (2)$$

It is possible to perform effective braking which provides both safety and better ride comfort by establishing a braking strategy according to the risk of collision because greater braking forces are required as the risk of collision increases. Therefore, we set two braking criteria ($\mathrm{TTC}_{\mathrm{brake}}$ and $\mathrm{TTC}_{\mathrm{emerg}}$) and compared the two braking criteria with the TTC* to determine the driving situation (see Figure 3). This decision process is performed for every time step (Δt) that acquired the motion data of the vehicles. In this study, 0.002 s was used for Δt. $\mathrm{TTC}_{\mathrm{brake}}$ and $\mathrm{TTC}_{\mathrm{emerg}}$ are the criteria for determining when smooth braking and when emergency braking are required, respectively. $\mathrm{TTC}_{\mathrm{emerg}}$ is set to a smaller time value than $\mathrm{TTC}_{\mathrm{brake}}$ because it is the criterion for discriminating a more dangerous driving situation as compared with $\mathrm{TTC}_{\mathrm{brake}}$.

In this study, the driving situation was classified into three cases according to TTC* and the two braking criteria. The first case is when TTC* is greater than $\mathrm{TTC}_{\mathrm{brake}}$. In this case, the possibility of a collision is very low. The second case is normal braking situation when TTC* is between $\mathrm{TTC}_{\mathrm{brake}}$ and $\mathrm{TTC}_{\mathrm{emerg}}$. In this case, it is effective to perform partial braking considering not only safety but also ride comfort because there is potential collision. In partial braking, smooth brake pressure that restores TTC* is applied because smoother braking results in less deceleration and jerk for a more comfortable ride (Martin and Litwhiler, 2008; Elbanhawi *et al*., 2015). The last case is emergency braking situation when TTC* is smaller than $\mathrm{TTC}_{\mathrm{emerg}}$. In this case, the possibility of collision is very high and full braking is performed to maximize the braking force.

2.2. Partial Braking Algorithm

Partial braking, which is the key control algorithm for the

smooth braking technique, is composed of a recovery zone and a release zone (see Figure 4). The former is the section when the brake pressure is smoothly applied to the following vehicle to recover the TTC^* to greater than TTC_{brake} and the latter is the section when the braking force is smoothly released to minimize the jerk of the vehicle when removing the brake pressure to improve ride comfort. In the recovery zone, where TTC^* is smaller than TTC_{brake}, the required brake pressure to restore TTC^* to the target value is calculated and it is applied to the vehicle during Δt_{rec}. In the release zone, when TTC^* has increased above TTC_{brake}, the brake pressure is removed during Δt_{rel} because brake control is no longer required to avoid the collision. However, if the brake pressure is instantaneously removed, a large jerk is generated causing discomfort for a driver. To attenuate discomfort in the release zone, the brake pressure is slowly removed. The recovery brake pressure is applied repeatedly until TTC^* exceeds TTC_{brake}, whereas the brake pressure is released after the completion of the recovery braking. In addition, in the release zone, if TTC^* again becomes smaller than TTC_{brake}, the recovery braking is resumed. Figure 5 illustrates the flow chart for the partial braking strategy.

The structure of the recovery and release braking algorithms consists of calculating the smooth brake pressure to achieve each target and applying the calculated brake pressure. The recovery braking algorithm involves additional computation processing as compared to the release braking algorithm because it calculates the brake pressure level in consideration of the TTC, whereas while in the case of release braking, the computation process is more concise because the goal is only to eliminate the brake pressure. This section describes how to calculate the recovery brake pressure by dividing into four subsections. At the end of the fourth subsection, the calculation method of release brake pressure is explained.

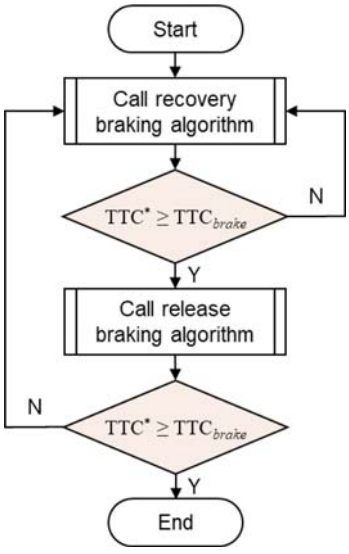

Figure 5. Flow chart of the partial braking algorithm.

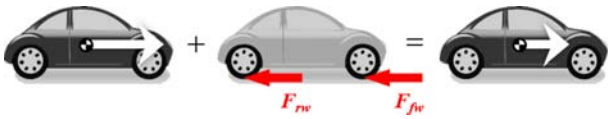

Figure 6. Application of principle of linear impulse and momentum to vehicle.

2.2.1. Behavior of following vehicle for recovery braking
The first step of the recovery braking algorithm is to calculate the displacement, velocity, and acceleration of the following vehicle. In the recovery zone, the behavior of the following vehicle could be determined by the expected behavior of the preceding vehicle and TTC(t), the predicted recovery curve for the TTC. In this study, the acceleration of the preceding vehicle was predicted by extrapolation and a second order polynomial was used to reflect the nonlinear behavior. Furthermore, the velocity and displacement of the preceding vehicle were obtained by integrating the predicted acceleration. For ride comfort, the following vehicle should be controlled to smoothly recover the TTC, so several conditions are considered to determine the TTC(t) as a smooth profile. Those considerations include the initial value, initial slope, final value, final slope, and recovery time, Δt_r.

The value of TTC(t_0) was calculated using Equation (2) and the slope of TTC(t_0) was extracted from the values of TTC^* at ($t_0 - \Delta t$) and t_0 in order to maintain continuous motion of the vehicle (refer to Figure 4). The value of TTC ($t_0 + \Delta t_{rec}$) at the end of recovery braking was set as the target value, TTC_{brake}, and the slope of TTC ($t_0 + \Delta t_{rec}$) was set at zero for a smooth TTC profile. In this study, recovery time, Δt_{rec} is set at 0.5 s. If the following vehicle does not recover the TTC_{brake} for recovery in this time, the recovery braking algorithm is repeated (see Figure 5).

To calculate the behavior of the following vehicle, we utilized Equation (2). In the recovery zone, Equation (2) can be rearranged for the displacement, velocity, and acceleration of the following vehicle by applying the predicted behavior of preceding vehicle and TTC(t). Then, as the velocities and accelerations are the derivative of the displacements and velocities with respect to the time, respectively, Equation (2) can be expressed as a linear differential equation. In order to solve the linear differential equation, we used the MATLAB ode45 solver based on the explicit Runge-Kutta method.

2.2.2. Calculation of braking force for recovery braking
Various forces acting on the moving vehicle were considered in the calculation of the braking forces to control the following vehicle. The longitudinal forces involved in the calculation were the forces acting on the front and rear wheels of the vehicle, the aerodynamic force, and the force due to gravity (Gillespie, 1992). The braking force of the following vehicle to achieve recovery braking was extracted using the principles of linear impulse and

momentum and can be expressed as follows.

$$m_{\text{vehicle}} v_{\text{t}} + \int_{\text{t}}^{\text{t}+\Delta\text{t}} \Sigma F \, dt = m_{\text{vehicle}} v_{\text{t}+\Delta\text{t}} \quad (t_0 \le t \le t_0 + \Delta t_{\text{rec}}) \quad (3)$$

where

$$\Sigma F = F_{\text{fw}} + F_{\text{rw}} - D_{\text{a}} - m_{\text{vehicle}} g \sin\theta$$
$$D_{\text{a}} = \frac{1}{2} A D C_{\text{d}} v_{\text{a}}^{\,2} \quad (4)$$

where m_{vehicle}, g, and θ are the mass of vehicle, acceleration of gravity, and uphill grade, respectively. F_{fw} and F_{rw} represent the longitudinal forces acting on the front and rear wheels transmitted from the road surface, respectively. Additionally, D_{a}, A, D, and C_{d} are the aerodynamic drag force, the frontal area of the vehicle, the air mass density, and the drag coefficient, respectively. The values used in this study are listed in Table 1. The v_{a} represents the relative speed between the vehicle and the air.

During braking, the braking force is expressed as the sum of the longitudinal forces acting on the front and rear wheels (see Figure 6). Therefore, the braking force required to achieve recovery braking was calculated by rearranging Equation (3) for F_{fw} and F_{rw}, and then differentiating both sides with respect to time as shown in Equation (5).

$$F_{\text{fw}}\big|_{\text{t}} + F_{\text{rw}}\big|_{\text{t}} = D_{\text{a}}\big|_{\text{t}} + m_{\text{vehicle}} g \sin\theta + m_{\text{vehicle}} \left.\frac{dv}{dt}\right|_{\text{t}} \quad (5)$$

2.2.3. Estimation of slip ratio and wheel angular velocity
In order to calculate the brake pressure required to achieve recovery braking, the nonlinear characteristics of the braking force with respect to the longitudinal slip ratio were considered. The Pacejka tire model and combined slip theory were used to calculate the braking force (Mechanical Simulation Corp., 2014). This model provides data on the longitudinal force as a function of the slip ratio (see Figure 7). The definition of slip ratio is as follows.

Table 1. Specification of the test vehicle.

Symbol	Quantity	Value	Unit
m_{vehicle}	Empty vehicle mass	1830	kg
I_{wheel}	Mass moment of inertia of wheel	0.9	kg·m^2
r	Effective rolling radius of tire	353	mm
G	Brake torque/pressure coefficient	250	N·m/MPa
A	Frontal area of vehicle	2.8	m^2
D	Air mass density	1.206	kg/m^3
C_{d}	Drag coefficient of vehicle	0.3	Dimension-less

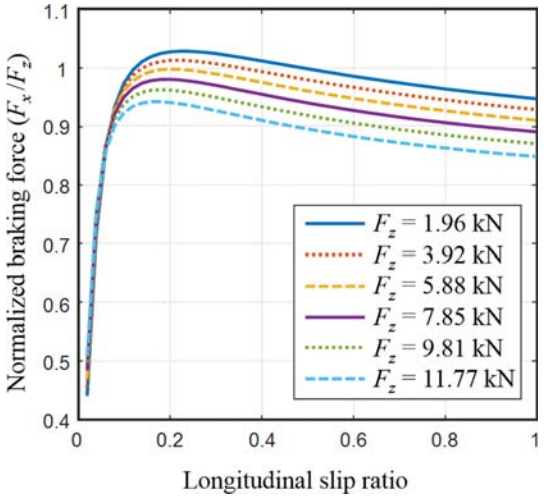

Figure 7. Braking forces with respect to slip ratio for several vertical forces obtained from CarSim software.

$$slip\ ratio = \frac{v - r\omega}{v} \quad (6)$$

where r is the effective rolling radius of a tire, ω is the angular velocity of a wheel, and v is the longitudinal velocity at the center of the wheel. The slip ratio was extracted using the relationship between slip ratio and braking force curves to obtain the calculated braking force (see Figure 7), and it was used for the calculation of the wheel angular velocity. The angular velocity of a wheel can be calculated using Equation (6), and it was then used to calculate the recovery brake pressure.

2.2.4. Calculation of recovery/release brake pressure
Various torques acting on the wheel were considered when calculating the brake pressure for vehicle control to satisfy the TTC profile. These torques included the engine shaft torque, braking torque, rolling resistance torque, and the torque generated by the longitudinal forces acting on the tire. In order to calculate the recovery brake pressure, we used the principle of angular impulse and momentum as following (see Figure 8).

$$I_{\text{wheel}}\, \omega_{\text{t}_0} + \int_{\text{t}_0}^{\text{t}_0+\Delta\text{t}_{\text{rec}}} \Sigma T \, dt = I_{\text{wheel}}\, \omega_{\text{t}_0+\Delta\text{t}_{\text{rec}}} \quad (7)$$

where

$$\Sigma T = T_{\text{s}} - T_{\text{b}} - T_{\text{rr}} - rF_{\text{x}} \quad (8)$$

where I_{wheel} is the mass moment of inertia of the wheel including the tire. T_{rr} is a function of the vehicle speed and T_{s} is a function of the engine throttle and engine speed (Mechanical Simulation Corp, 2014). T_{b} is the brake torque and is proportional to $P(t)$ which is the brake pressure of the master cylinder. This relationship is expressed as follows.

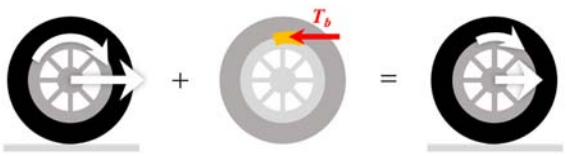

Figure 8. Application of principle of angular impulse and momentum to vehicle.

$$T_b(t) = G \cdot P(t) \tag{9}$$

where G is the brake pressure-torque coefficient set to 250 N·m/MPa in this study. A smooth recovery brake pressure was required because a large jerk generates poor ride comfort when a sudden brake pressure such as a step is applied to the vehicle. Therefore, several conditions are considered to obtain the smooth brake pressure. Those conditions include the initial value, the initial slope, the final slope, and the integral of pressure over time. The $P(t_0)$ was extracted using the brake pressure applied to the vehicle prior to t_0 and the slopes of $P(t_0)$ and $P(t_0 + \Delta t_{rec})$ were set to zero to minimize the change in brake pressure. In addition, the brake pressure to achieve the recovery braking should satisfy Equation (7). To consider four conditions, the brake pressure profile was determined to be a cubic function. The function of smooth brake pressure to be applied to the following vehicle and the conditions for achieving recovery braking are as follows.

$$P(t) = c_0 t^3 + c_1 t^2 + c_2 t + c_3 \quad (t_0 \le t \le t_0 + \Delta t_{rec}) \tag{10}$$

Conditions for recovery braking:

$$\begin{cases} P(t_0) = 2P^*(t_0 - \Delta t) - P^*(t_0 - 2\Delta t) \\ \left.\dfrac{dP(t)}{dt}\right|_{t_0} = 0 \\ G\displaystyle\int_{t_0}^{t_0+\Delta t_{rec}} P(t)\,dt = I_{wheel}(\omega_{t_0+\Delta t_{rec}} - \omega_{t_0}) + \int_{t_0}^{t_0+\Delta t_{rec}} (T_s - T_{rr} - rF_x)\,dt \\ \left.\dfrac{dP(t)}{dt}\right|_{t_0+\Delta t_{rec}} = 0 \end{cases} \tag{11}$$

where P^* is the brake pressure before t_0. In addition, the fluid dynamics time constant was considered to calculate the brake pressure considering the time delay caused by the fluid dynamics in the brake chamber. This time constant was set to 0.06 s in this study.

In order to consider ride comfort in release braking, the conditions for calculating the release brake pressure were determined similar to the conditions for recovery braking. Because the third condition in Equation (11) was for the recovery of TTC, it was replaced with a zero brake pressure condition at the end of the release period. In addition, in this study, the release time, Δt_{rel}, was set to 2 s but this value could be adjusted to improve the ride comfort of the vehicle. With the time at which TTC* is recovered to TTC_{brake} referred to as $\hat{t}_0$ (see Figure 4), the conditions for achieving release braking are as follows.

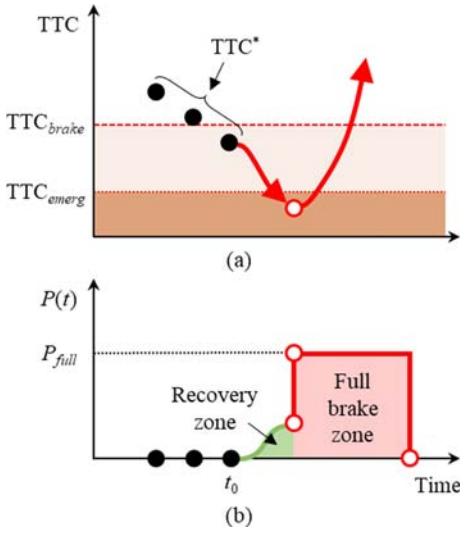

Figure 9. Conceptual diagram of the full braking algorithm: (a) TTC*; (b) Corresponding brake pressure.

Conditions for release braking:

$$\begin{cases} P(\hat{t}_0) = 2P(\hat{t}_0 - \Delta t) - P(\hat{t}_0 - 2\Delta t) \\ \left.\dfrac{dP(t)}{dt}\right|_{\hat{t}_0} = 0 \\ P(\hat{t}_0 + \Delta t_{rel}) = 0 \\ \left.\dfrac{dP(t)}{dt}\right|_{\hat{t}_0+\Delta t_{rel}} = 0 \end{cases} \tag{12}$$

In summary, the procedures for the calculation of the brake pressure is summarized as follows:

(1) Calculate the braking force satisfying TTC
(2) Extract the slip ratio from the calculated braking force and the relationship between the braking force and slip ratio (see Figure 7)
(3) Calculate the wheel angular velocity using the extracted slip ratio from Equation (6) at the vehicle's speed
(4) Calculate brake pressure using the calculated wheel angular velocity and Equations (7) ~ (10).

2.3. Full Braking Algorithm

Finally, the full braking algorithm for emergency avoidance is also included in the study. In a dangerous situation such as an impending accident or sudden braking by the preceding vehicle, the partial braking technique could not perform a rapid enough recovery of the TTC* and, therefore, it might increase the risk of collision. In order to cope with an emergency, a brake control algorithm that prioritizes the safety of the vehicle is required.

The full braking algorithm proposed in this paper controls the vehicle to perform sudden braking beginning the moment when TTC* becomes smaller than TTC_{emerg} (see Figure 9). In situations where full braking is required, we controlled the vehicle to apply full brake pressure in the

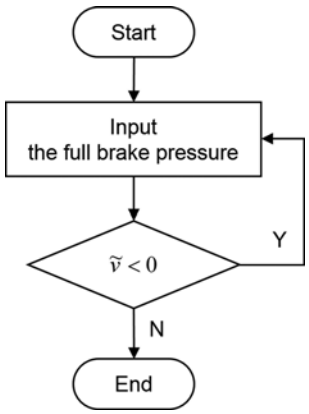

Figure 10. Flow chart of the full braking algorithm.

form of a step function to minimize the distance lost between the two vehicles. Then, if the velocity of the following vehicle becomes less than that of the preceding vehicle, the vehicle-to-vehicle distance increases and the collision does not occur, thus full brake pressure will be eliminated when the relative velocity is greater than zero (see Figure 10). To evaluate the system response performance of the proposed braking algorithm, a vehicle without an anti-lock braking system (ABS) was used and the full brake pressure was set to be applied at maximum pressure for the test vehicle.

3. SIMULATION METHOD AND RESULTS

In order to verify the performance of the proposed autonomous braking system, numerical simulations with two driving scenarios were performed. The vehicle model of the following vehicle used for the simulation is an E-Class sedan and the detailed specifications of the vehicle model are shown in Table 1. In this study, a smooth, dry road without slope was selected and the coefficient of friction between the tire and the road surface was set at 1.0. The CarSim and MATLAB/Simulink were used for the simulations and the braking control algorithm was implemented with the MATLAB/Simulink model.

3.1. Partial Braking Scenrio

In order to verify the performance of the partial braking algorithm, a simulation was performed for a scenario in which the preceding vehicle is slowly decelerating from high speed. The initial speed of both vehicles was set at 110 km/h and the initial relative distance was set at 50 m. In this study, we set the TTC_{brake} to 5 s for the braking criterion and implemented the driving situation in which the preceding vehicle decelerates twice to 90 km/h and 80 km/h.

Figure 11 shows the velocity, TTC^*, brake pressure, acceleration, and jerk over a period of 10 s. As can be seen in Figure 11 (d), the accelerations of the following vehicle controlled by the proposed braking algorithm are changed

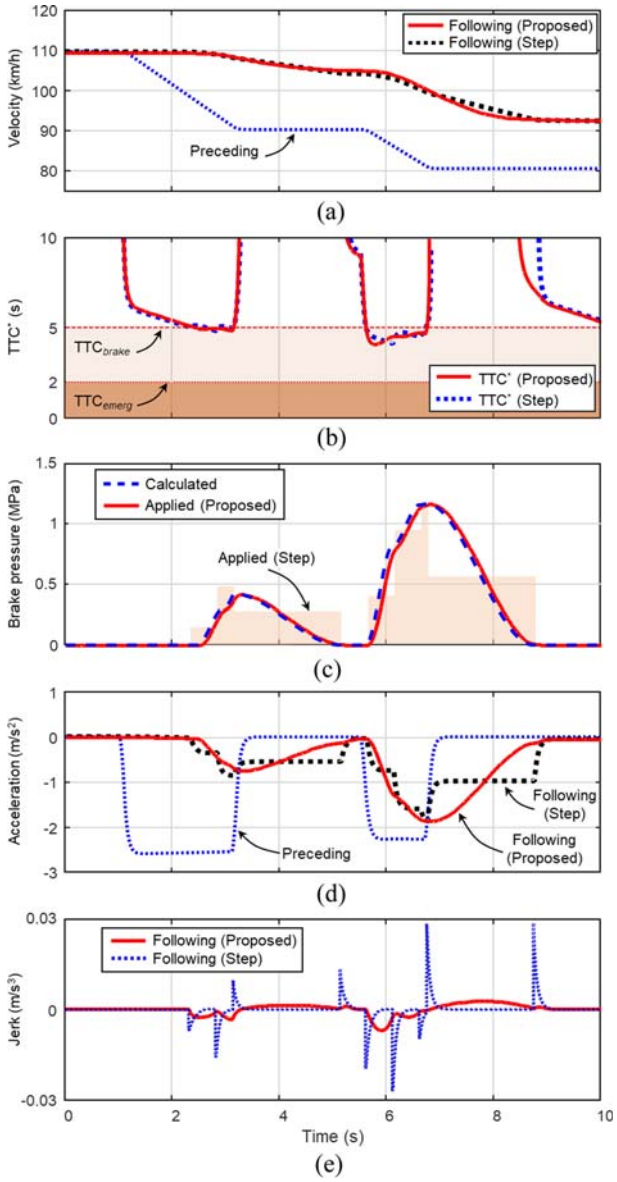

Figure 11. Simulation results on the partial braking scenario: (a) Velocity; (b) TTC^*; (c) Brake pressure of the following vehicle; (d) Acceleration; (e) Jerk of the following vehicles.

more smoothly. Using the profiles of the braking pressure with the step function type, there are fluctuations in the accelerations of the following vehicle when the accelerations are decrease. The proposed braking strategy has lower jerks than the braking algorithm using the stiff braking pressure.

When the preceding vehicle started to brake, the TTC^* sharply decreased due to the change in the acceleration of the preceding vehicle (see Figures 11 (b) and (d)). After that point, the deceleration of the preceding vehicle became a constant at about 2.55 m/s^2 and the slope of the TTC^* decreased at the same time. At approximately 2.5 s, the

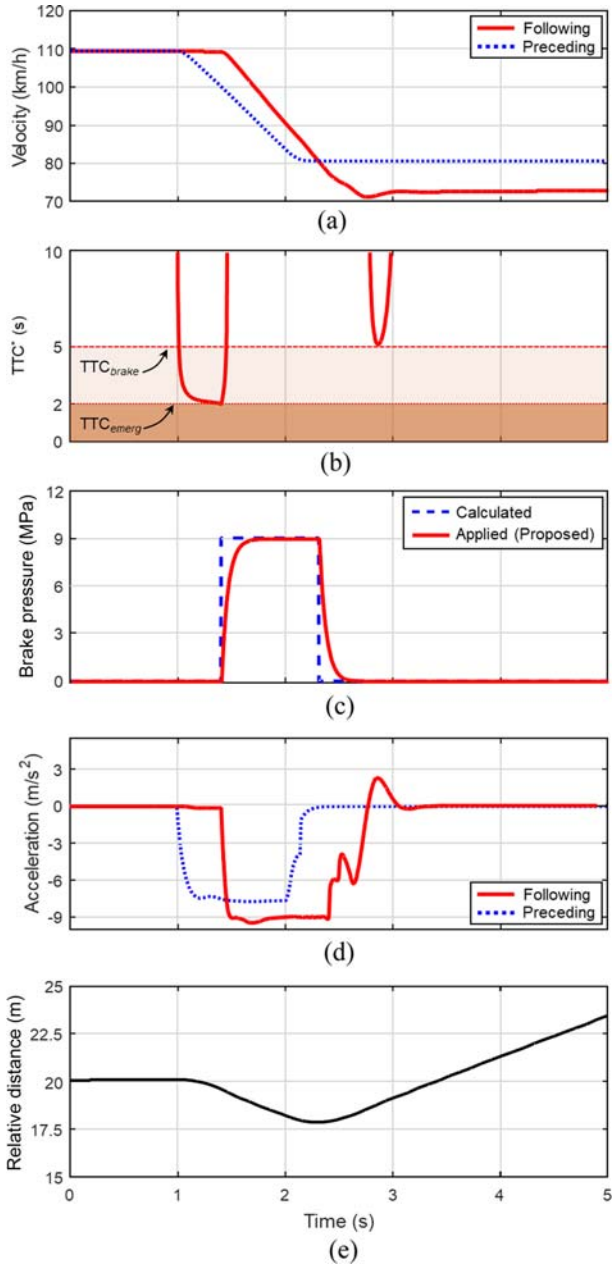

Figure 12. Simulation results on the full braking scenario: (a) Velocity of the test vehicles; (b) TTC*; (c) Brake pressure of the following vehicle; (d) Acceleration of the test vehicles; (e) Relative distance between preceding and following vehicles.

partial braking control was started when TTC* became smaller than TTC_{brake} (see Figure 11 (c)). The brake pressure was calculated from the recovery braking algorithm, but in the actual simulation, the applied pressure acts a little later than the calculated pressure because there is some time delay in the hydraulic brake system. Then, it could be confirmed that TTC* did not decrease any further due to the recovery braking and recovered to TTC_{brake}. The moment the preceding vehicle resumes the constant speed motion after finishing the first brake, the deceleration of the preceding vehicle decreases and the TTC* increases greatly. Furthermore, the recovery braking algorithm was completed and the release braking algorithm was activated due to TTC* being larger than TTC_{brake}. As a result, the deceleration of the following vehicle was gradually reduced so that the vehicle behavior for good ride comfort could be obtained.

The results during the second deceleration by the preceding vehicle are generally similar to the results of the first deceleration period. However, there are two noteworthy differences compared to the results of the first deceleration. One difference is that the TTC* was smaller than the TTC_{brake} immediately after the preceding vehicle started to decelerate. The other difference is that in the second deceleration a higher recovery brake pressure was calculated even though the preceding vehicle had a lower deceleration (approximately 2.25 m/s^2) compared to the first deceleration. The reason for these differences was that a larger braking force was required because the relative distance between the two vehicles was smaller than the initial relative distance of the first braking. Nonetheless, the TTC* recovered to the TTC_{brake} in the second deceleration interval. This indicates that the partial braking algorithm operates successfully even in different driving situations.

Through this simulation, it was confirmed that the deceleration of the following vehicle is remarkably smaller than that of the preceding vehicle whereas the relative distance between the two vehicles is continuously decreased. These results show that not only was there adequate braking performance but the ride comfort was also successfully considered by the application of the partial braking algorithm.

3.2. Full Braking Scenario

In order to verify the performance of the full braking algorithm, a simulation was performed for a scenario in which the driver of the preceding vehicle brakes suddenly while traveling at a high speed. The initial speed of the two vehicles was set at 110 km/h and the initial relative distance was set at 20 m. Figure 12 shows the simulation results for the full braking scenario. TTC_{brake} was set to 5 s, the same as in the partial braking scenario and TTC_{emerg} was set to 2 s.

Immediately after the preceding vehicle started to decelerate, the TTC* decreased vertically and became smaller than the TTC_{brake} (see Figures 12 (b) and (d)). Then, the partial braking algorithm was operated for about 0.4 s but the TTC* decreased continuously because the braking force was insufficient to recover the TTC*. When the TTC* reached the TTC_{emerg}, the full braking algorithm was initiated (see Figures 12 (b) and (c)). The TTC* quickly recovered by applying full brake pressure to the following vehicle. However, in order to fully cope with the emergency, the following vehicle was controlled to

continuously apply the full brake pressure until the following vehicle speed became smaller than that of the preceding vehicle.

As a result, the full braking was terminated at about 2.31 s when the speed of the following vehicle became less than the speed of the preceding vehicle. Following that point, there was no brake control but due to the fluctuation of the following vehicle's deceleration, the TTC^* decreased and then increased again (see Figures 12 (b) ~ (d)). The reason for this is that a pitch motion occurred due to the absence of the release braking algorithm. The full braking algorithm does not include a release braking algorithm because it focuses on safe braking rather than ride comfort.

Similar to the results of the partial braking scenario, the actual brake pressure application was later than the calculated brake pressure due to the time delay of the hydraulic brake system (see Figure 12 (c)). In Figure 12 (e), the relative distance decreased by about 2.4 m during the full braking but increased again after the full braking was completed. This means that collision was successfully avoided by applying the full braking algorithm in the sudden braking situation of the preceding vehicle and, furthermore, by ensuring the relative distance is kept beyond the safety distance, the control algorithm was designed to put safety as the top priority.

4. CONCLUSION

We developed an autonomous braking algorithm that determines the driving situation to secure the safety of the vehicle and to provide improved ride comfort. The braking algorithm was designed to estimate the driving situation of the vehicle using the TTC calculated from the relative distance, speed, and acceleration between the preceding and following vehicles as well as to provide improved ride comfort by adopting the required braking strategy for each driving situation. The proposed algorithm was verified by the simulation results with several driving situations using CarSim and MATLAB/Simulink. The driving situations were selected as scenarios in which each braking strategy could be performed and the performance of the braking algorithms according to each scenario was analyzed. The results show that the partial braking algorithm not only guarantees the safety of the vehicle but also provides an improved ride comfort. In addition, we confirmed that the full braking algorithm could be used to avoid a collision in an emergency scenario. Furthermore, from the results of the simulations, we could observed that the change in TTC^* is sensitive to changes in the acceleration of two vehicles. This is the result of considering the acceleration in the TTC calculation, which means that the braking algorithm based on TTC^* is able to quickly detect the risk of a collision due to the deceleration of the preceding vehicle.

ACKNOWLEDGEMENT–This research was supported by the MSIP (Ministry of Science, ICT and Future Planning), Korea, under the ITRC (Information Technology Research Center) (IITP-2016-H8601-16-1002) supervised by the IITP (Institute for Information & communications Technology Promotion).

REFERENCES

Elbanhawi, M., Simic, M. and Jazar, R. (2015). In the passenger seat: Investigating ride comfort measures in autonomous cars. *IEEE Intelligent Transportation Systems Magazine* **7**, **3**, 4–17.

Erdogan, G., Alexander, L. and Rajamani, R. (2011). Estimation of tire-road friction coefficient using a novel wireless piezoelectric tire sensor. *IEEE Sensors J.* **11**, **2**, 267–279.

Ferrara, A. and Claudio, V. (2007). Collision avoidance strategies and coordinated control of passenger vehicles. *Nonlinear Dynamics* **49**, **4**, 475–492.

Gillespie, T. D. (1992). *Fundamentals of Vehicle Dynamics*. SAE International. Pittsburgh, Pennsylvania, USA.

Gustafsson, F. (1997). Slip-based tire-road friction estimation. *Automatica* **33**, **6**, 1087–1099.

Hahn, J. O., Rajamani, R. and Alexander, L. (2002). GPS-based real-time identification of tire-road friction coefficient. *IEEE Trans. Control Systems Technology* **10**, **3**, 331–343.

Hayashi, R., Isogai, J., Raksincharoensak, P. and Nagai, M. (2012). Autonomous collision avoidance system by combined control of steering and braking using geometrically optimised vehicular trajectory. *Vehicle System Dynamics: Int. J. Vehicle Mechanics and Mobility* **50**, **Supplement 1**, 151–168.

Isermann, R. and Schmitt, K. (2012). Collision-avoidance systems PRORETA: Situation analysis and intervention control. *Control Engineering Practice* **20**, **11**, 1236–1246.

Kim, D. J., Park, K. H. and Bien, Z. (2007). Hierarchical longitudinal controller for rear-end collision avoidance. *IEEE Trans. Industrial Electronics* **54**, **2**, 805–817.

Kusano, K. D. and Gabler, H. C. (2012). Safety benefits of forward collision warning, brake assist, and autonomous braking systems in rear-end collisions. *IEEE Trans. Intelligent Transportation Systems* **13**, **4**, 1546–1555.

Martin, D. and Litwhiler, D. (2008). An investigation of acceleration and jerk profiles of public transportation vehicles. *Proc. ASEE Annual Conf. and Exposition*, Pittsburgh, Pennsylvania, USA.

Mechanical Simulation Corp (2014). CarSim User Manual Ver. 9.0.

Milanés, V., Pérez, J., Godoy, J. and Onieva, E. (2012). A fuzzy aid rear-end collision warning/avoidance system. *Expert Systems with Applications* **39**, **10**, 9097–9107.

Moon, S. and Yi, K. (2008). Human driving data-based design of a vehicle adaptive cruise control algorithm. *Vehicle System Dynamics: Int. J. Vehicle Mechanics and Mobility* **46**, **8**, 661–690.

Naranjo, J. E., González, C., Reviejo, J., García, R. and Pedro, T. D. (2003). Adaptive fuzzy control for inter-vehicle gap keeping. *IEEE Trans. Intelligent Transportation Systems* **4**, **3**, 132–142.

Naranjo, J. E., Jiménez, F., Gómez, O. and Zato, J. G. (2012). Low level control layer definition for autonomous vehicles based on fuzzy logic. *Intelligent Automation and Soft Computing* **18**, **4**, 333–348.

NHTSA (2018). Traffic Safety Facts 2016: A Compilation of Motor Vehicle Crash Data from the Fatality Analysis Reporting System and the General Estimates System. NHTSA Annual Report. DOT HS 812 554.

Savaresi, S. M. and Tanelli, M. (2010). *Active Braking Control Systems Design for Vehicles*. Springer. London, UK.

Sengupta, R., Rezaei, S., Shladover, S. E., Cody, D., Dickey, S. and Krishnan, H. (2007). Cooperative collision warning systems: Concept definition and experimental implementation. *J. Intelligent Transportation Systems* **11**, **3**, 143–155.

Sivaraman, S. and Trivedi, M. M. (2013). Looking at vehicles on the road: A survey of vision-based vehicle detection, tracking, and behavior analysis. *IEEE Trans. Intelligent Transportation Systems* **14**, **4**, 1773–1795.

Vogel, K. (2003). A comparison of headway and time to collision as safety indicators. *Accident Analysis and Prevention* **35**, **3**, 427–433.

Wu, Z., Liu, Y. and Pan, G. (2009). A smart car control model for brake comfort based on car following. *IEEE Trans. Intelligent Transportation Systems* **10**, **1**, 42–46.

Yang, I. B., Na, S. G. and Heo, H. (2017). Intelligent algorithm based on support vector data description for automotive collision avoidance system. *Int. J. Automotive Technology* **18**, **1**, 69–77.

Yi, K. and Chung, J. T. (2001). Nonlinear brake control for vehicle CW/CA systems. *IEEE/ASME Trans. Mechatronics* **6**, **1**, 17–25.